

Tunable Q-switched fiber laser based on saturable edge-state absorption in few-layer molybdenum disulfide (MoS₂)

R. I. Woodward,^{1,*} E. J. R. Kelleher,¹ R. C. T. Howe,² G. Hu,²
F. Torrisi,² T. Hasan,² S. V. Popov¹ and J. R. Taylor¹

¹Femtosecond Optics Group, Department of Physics, Imperial College London, SW7 2AZ, UK

²Cambridge Graphene Centre, University of Cambridge, Cambridge, CB3 0FA, UK

*r.woodward12@imperial.ac.uk

Abstract: We fabricate a few-layer molybdenum disulfide (MoS₂) polymer composite saturable absorber by liquid-phase exfoliation, and use this to passively Q-switch an ytterbium-doped fiber laser, tunable from 1030 to 1070 nm. Self-starting Q-switching generates 2.88 μs pulses at 74 kHz repetition rate, with over 100 nJ pulse energy. We propose a mechanism, based on edge states within the bandgap, responsible for the wideband nonlinear optical absorption exhibited by our few-layer MoS₂ sample, despite operating at photon energies lower than the material bandgap.

© 2014 Optical Society of America

OCIS codes: (140.3510) Lasers, fiber; (140.3540) Lasers, Q-switched; (160.4236) Nanomaterials; (160.4330) Nonlinear optical materials.

References and links

1. Q. H. Wang, K. Kalantar-Zadeh, A. Kis, J. N. Coleman, and M. S. Strano, "Electronics and optoelectronics of two-dimensional transition metal dichalcogenides," *Nat. Nanotechnol.* **7**, 699–712 (2012).
2. R. F. Frindt, "Optical absorption of a few unit-cell layers of MoS₂," *Phys. Rev.* **140**, A536–A539 (1965).
3. P. Joensen, R. F. Frindt, and S. R. Morrison, "Single-layer MoS₂," *Mater. Res. Bull.* **21**, 457–461 (1986).
4. K. F. Mak, C. Lee, J. Hone, J. Shan, and T. F. Heinz, "Atomically thin MoS₂: a new direct-gap semiconductor," *Phys. Rev. Lett.* **105**, 136805–1 (2010).
5. C. B. Roxlo, M. Daage, A. F. Ruppert, and R. R. Chianelli, "Optical absorption and catalytic activity of molybdenum sulfide edge surfaces," *J. Catal.* **100**, 176–184 (1986).
6. C. B. Roxlo, M. Daage, D. P. Leta, K. S. Liang, S. Rice, A. F. Ruppert, and R. R. Chianelli, "Catalytic defects at molybdenum disulfide "edge" planes," *Solid State Ionics* **22**, 97–104 (1986).
7. C. B. Roxlo, "Bulk and surface optical absorption in molybdenum disulfide," *J. Vac. Sci. Technol. A* **5**, 555–557 (1987).
8. S. Kasap, *Principles of Electronic Materials and Devices* (McGraw-Hill, 2005).
9. P. Yu and M. Cardona, *Fundamentals of Semiconductors: Physics and Materials Properties* (Springer, 2010).
10. K. Wang, J. Wang, J. Fan, M. Lotya, A. O'Neill, D. Fox, Y. Feng, X. Zhang, B. Jiang, Q. Zhao, H. Zhang, J. N. Coleman, L. Zhang, and W. J. Blau, "Ultrafast saturable absorption of two-dimensional MoS₂ nanosheets," *ACS Nano* **7**, 9260–9267 (2013).
11. K. Wang, Y. Feng, C. Chang, J. Zhan, C. Wang, Q. Zhao, J. N. Coleman, L. Zhang, W. Blau, and J. Wang, "Broadband ultrafast nonlinear absorption and nonlinear refraction of layered molybdenum dichalcogenide semiconductors," *Nanoscale* **6**, 10530–10535 (2014).
12. Q. Ouyang, H. Yu, K. Zhang, and Y. Chen, "Saturable absorption and the changeover from saturable absorption to reverse saturable absorption of MoS₂ nanoflake array films," *J. Mater. Chem. C* **2**, 6319–6325 (2014).
13. H. Zhang, S. B. Lu, J. Zheng, J. Du, S. C. Wen, D. Y. Tang, and K. P. Loh, "Molybdenum disulfide (MoS₂) as a broadband saturable absorber for ultra-fast photonics," *Opt. Express* **22**, 7249–7260 (2014).
14. J. Du, Q. Wang, G. Jiang, C. Xu, C. Zhao, Y. Xiang, Y. Chen, S. Wen, H. Zhang, "Ytterbium-doped fiber laser passively mode locked by few-layer Molybdenum Disulfide (MoS₂) saturable absorber functioned with evanescent field interaction," *Sci. Rep.* **4**, 6346 (2014).

15. H. Xia, H. Li, C. Lan, C. Li, X. Zhang, S. Zhang, and Y. Liu, "Ultrafast erbium-doped fiber laser mode-locked by a CVD-grown molybdenum disulfide (MoS₂) saturable absorber," *Opt. Express* **22**, 17341–17348 (2014).
16. H. Liu, A.-P. Luo, F.-Z. Wang, R. Tang, M. Liu, Z.-C. Luo, W.-C. Xu, C.-J. Zhao, and H. Zhang, "Femtosecond pulse erbium-doped fiber laser by a few-layer MoS₂ saturable absorber," *Opt. Lett.* **39**, 4591–4594 (2014).
17. R. Khazaiezhad, S. H. Kassani, H. Jeong, D.-I. Yeom, K. Oh, "Mode-locking of Er-doped fiber laser using a multilayer MoS₂ thin film as a saturable absorber in both anomalous and normal dispersion regimes," *Opt. Express* **22**, 23732–23742 (2014).
18. S. Wang, H. Yu, H. Zhang, A. Wang, M. Zhao, Y. Chen, L. Mei, and J. Wang, "Broadband few-layer MoS₂ saturable absorbers," *Adv. Mater.* **26**, 3538–3544 (2014).
19. R. I. Woodward, E. J. Kelleher, T. H. Runcorn, S. V. Popov, F. Torrisi, R. T. Howe, and T. Hasan, "Q-switched fiber laser with MoS₂ saturable absorber," in *CLEO: 2014, OSA Technical Digest (Optical Society of America, 2014)*, paper SM3H-6.
20. R. Wang, H.-C. Chien, J. Kumar, N. Kumar, H.-Y. Chiu, and H. Zhao, "Third-harmonic generation in ultrathin films of MoS₂," *ACS Appl. Mater. Interfaces* **6**, 314–318 (2014).
21. R. Wang, B. a. Ruzicka, N. Kumar, M. Z. Bellus, H.-Y. Chiu, and H. Zhao, "Ultrafast and spatially resolved studies of charge carriers in atomically thin molybdenum disulfide," *Phys. Rev. B* **86**, 045406 (2012).
22. Y. Huang, Z. Luo, Y. Li, M. Zhong, B. Xu, K. Che, H. Xu, Z. Cai, J. Peng, J. Weng, "Widely-tunable, passively Q-switched erbium-doped fiber laser with few-layer MoS₂ saturable absorber," *Opt. Express* **22**, 25258–25266 (2014).
23. X. Yin, Z. Ye, D. A. Chenet, Y. Ye, K. O'Brien, J. C. Hone, and X. Zhang, "Edge nonlinear optics on a MoS₂ atomic monolayer," *Science* **344**, 488–490 (2014).
24. M. I. Demchuk, N. V. Kuleshov, and V. P. Mikhailov, "Saturable absorbers based on impurity and defect centers in crystals," *IEEE J. Quant. Electron.* **30**, 2120–2126 (1994).
25. Z. Zhang, L. Qian, D. Fan, and X. Deng, "Gallium arsenide: A new material to accomplish passively mode-locked Nd:YAG laser," *Appl. Phys. Lett.* **60**, 419–421 (1992).
26. F. Bonaccorso, A. Lombardo, T. Hasan, Z. Sun, L. Colombo, and A. C. Ferrari, "Production and processing of graphene and 2d crystals," *Mater. Today* **15**, 564–589 (2012).
27. K.-K. Liu, W. Zhang, Y.-H. Lee, Y.-C. Lin, M.-T. Chang, C.-Y. Su, C.-S. Chang, H. Li, Y. Shi, H. Zhang, C.-S. Lai, and L.-J. Li, "Growth of large-area and highly crystalline MoS₂ thin layers on insulating substrates," *Nano Lett.* **12**, 1538–1544 (2012).
28. Y.-H. Lee, X.-Q. Zhang, W. Zhang, M.-T. Chang, C.-T. Lin, K.-D. Chang, Y.-C. Yu, J. T.-W. Wang, C.-S. Chang, L.-J. Li, and T.-W. Lin, "Synthesis of large-area MoS₂ atomic layers with chemical vapor deposition," *Adv. Mater.* **24**, 2320–2325 (2012).
29. Y.-H. Lee, L. Yu, H. Wang, W. Fang, X. Ling, Y. Shi, C.-T. Lin, J.-K. Huang, M.-T. Chang, C.-S. Chang, M. Dresselhaus, T. Palacios, L.-J. Li, and J. Kong, "Synthesis and transfer of single-layer transition metal disulfides on diverse surfaces," *Nano Lett.* **13**, 1852–1857 (2013).
30. G. Eda, H. Yamaguchi, D. Voiry, T. Fujita, M. Chen, and M. Chhowalla, "Photoluminescence from chemically exfoliated MoS₂," *Nano Lett.* **11**, 5111–5116 (2011).
31. J. N. Coleman, U. Khan, K. Young, A. Gaucher, S. De, R. J. Smith, I. V. Shvets, S. K. Arora, G. Stanton, H.-y. Kim, K. Lee, G. T. Kim, G. S. Duesberg, T. Hallam, J. J. Boland, J. J. Wang, J. F. Donegan, J. C. Grunlan, G. Moriarty, A. Shmeliov, R. J. Nicholls, J. M. Perkins, E. M. Grievson, K. Theuwissen, D. W. McComb, P. D. Nellist, and V. Nicolosi, "Two-dimensional nanosheets produced by liquid exfoliation of layered materials," *Science* **331**, 568–571 (2011).
32. F. Withers, H. Yang, L. Britnell, A. P. Rooney, E. Lewis, A. Felten, C. R. Woods, V. Sanchez Romaguera, T. Georgiou, A. Eckmann, Y. J. Kim, S. G. Yeates, S. J. Haigh, a. K. Geim, K. S. Novoselov, and C. Casiraghi, "Heterostructures produced from nanosheet-based inks," *Nano Lett.* **14**, 3987–3992 (2014).
33. G. Cunningham, M. Lotya, C. S. Cucinotta, S. Sanvito, S. D. Bergin, R. Menzel, M. S. P. Shaffer, and J. N. Coleman, "Solvent exfoliation of transition metal dichalcogenides: dispersibility of exfoliated nanosheets varies only weakly between compounds," *ACS Nano* **6**, 3468–3480 (2012).
34. J. N. Coleman, "Liquid-phase exfoliation of nanotubes and graphene," *Adv. Funct. Mater.* **19**, 3680–3695 (2009).
35. T. Hasan, F. Torrisi, Z. Sun, D. Popa, V. Nicolosi, G. Privitera, F. Bonaccorso, and A. C. Ferrari, "Solution-phase exfoliation of graphite for ultrafast photonics," *Phys. Status Solidi B* **247**, 2953–2957 (2010).
36. Y. Hernandez, M. Lotya, D. Rickard, S. D. Bergin, and J. N. Coleman, "Measurement of multicomponent solubility parameters for graphene facilitates solvent discovery," *Langmuir* **26**, 3208–13 (2010).
37. Z. Sun, D. Popa, T. Hasan, F. Torrisi, F. Wang, E. J. R. Kelleher, J. C. Travers, V. Nicolosi, and A. C. Ferrari, "A stable, wideband tunable, near transform-limited, graphene-mode-locked, ultrafast laser," *Nano Res.* **3**, 653–660 (2010).
38. Y. Hernandez, V. Nicolosi, M. Lotya, F. M. Blighe, Z. Sun, S. De, I. T. McGovern, B. Holland, M. Byrne, Y. K. Gun'Ko, J. J. Boland, P. Niraj, G. Duesberg, S. Krishnamurthy, R. Goodhue, J. Hutchison, V. Scardaci, A. C. Ferrari, and J. N. Coleman, "High-yield production of graphene by liquid-phase exfoliation of graphite," *Nat. Nanotechnol.* **3**, 563–8 (2008).
39. J. N. Israelachvili, *Intermolecular and Surface Forces* (Academic, 2011).

40. A. R. Beal, J. C. Knights, and W. Y. Liang, "Transmission spectra of some transition metal dichalcogenides. II. Group VIA: trigonal prismatic coordination," *J. Phys. C* **5**, 3540–3551 (1972).
 41. R. A. Bromley, R. B. Murray, and A. D. Yoffe, "The band structures of some transition metal dichalcogenides: III. Group VIA : trigonal prism materials," *J. Phys. C* **5**, 759–778 (1972).
 42. C. Lee, H. Yan, L. E. Brus, T. F. Heinz, J. Hone, and S. Ryu, "Anomalous lattice vibrations of single- and few-layer MoS₂," *ACS Nano* **4**, 2695–2700 (2010).
 43. T. Hasan, Z. Sun, F. Wang, F. Bonaccorso, P. H. Tan, A. G. Rozhin, and A. C. Ferrari, "Nanotube-polymer composites for ultrafast photonics," *Adv. Mater.* **21**, 3874–3899 (2009).
 44. C. F. Bohren and D. R. Huffman, *Absorption and Scattering of Light by Small Particles* (Wiley, 2007).
 45. M. Sheik-Bahae, A. A. Said, T.-H. Wei, D. Hagan, and E. Van Stryland, "Sensitive measurement of optical nonlinearities using a single beam," *IEEE J. Quant. Electron.* **26**, 760–769 (1990).
 46. E. Garmire, "Resonant optical nonlinearities in semiconductors," *IEEE J. Sel. Top. Quant. Electron.* **6**, 1094–1110 (2000).
 47. D. von der Linde, "Characterization of the noise in continuously operating mode-locked lasers," *Appl. Phys. B* **39**, 201–217 (1986).
 48. D. Popa, Z. Sun, T. Hasan, F. Torrisi, F. Wang, and A. C. Ferrari, "Graphene Q-switched, tunable fiber laser," *Appl. Phys. Lett.* **98**, 073106 (2011).
 49. J. Degnan, "Optimization of passively Q-switched lasers," *IEEE J. Quant. Electron.* **31**, 1890–1901 (1995).
 50. H. Shi, R. Yan, S. Bertolazzi, J. Brivio, B. Gao, A. Kis, D. Jena, H. G. Xing, and L. Huang, "Exciton Dynamics in Suspended 2D Crystals," *ACS Nano* **7**, 1072–1080 (2013).
-

1. Introduction

The emergence of graphene as a promising material for optoelectronic applications has triggered interest in other two-dimensional (2D) materials with distinct yet complementary electrical and optical properties. Within the layered material family, transition metal dichalcogenides (TMDs) have received the most attention, with their thickness-dependent optoelectronic properties when exfoliated to few layers from their bulk form. TMDs, such as molybdenum disulfide (MoS₂), are indeed ideal candidates for a wide range of optoelectronic applications, as evidenced by numerous recent demonstrations of MoS₂-based logic devices, photodetectors and light emitters [1].

In TMDs, two layers of chalcogen atoms (e.g. S) sandwich a layer of transition metal atoms (e.g. Mo), forming a trilayer sheet. Many of these sheets are stacked together by weak van der Waals forces, forming three-dimensional bulk TMDs. Such a structure allows exfoliation of single- or few-layer flakes from their bulk crystals [1].

The optical properties of bulk and thin crystals of MoS₂ are well documented [2–7]. Early studies reported observations of different behaviour of thin flakes from their bulk counterparts. In 1965, Frindt reported new features in the absorption spectrum of few-layer MoS₂ flakes, mechanically exfoliated using adhesive tape [2]. Twenty years later Joensen, Frindt and Morrison used lithium-based intercalation to obtain monolayers of the material [3]. Bulk MoS₂ is an indirect semiconductor with 1.29 eV (961 nm) bandgap which increases to a direct 1.80 eV (689 nm) bandgap for monolayers of the material [4]. In a perfect crystal, there is ideally no sub-bandgap absorption (corresponding to incident light with single-photon energy insufficient to excite electrons from the valence to conduction band) [8, 9]. However, in a finite system, boundary effects and edges can modify a crystal's absorption spectrum [8, 9]. The dependence of optical absorption on MoS₂ flake size was characterized using photothermal deflection spectroscopy at photon energies above and below the bandgap [5–7]. For energies above the bandgap, similar absorption spectra were observed for all samples. However, at sub-bandgap photon energies, a larger absorption was measured for flakes of MoS₂ (~36 μm in lateral diameter), which was up to an order of magnitude greater compared to single MoS₂ crystals [5–7]. Smaller flakes exhibited even stronger sub-bandgap absorption (two orders of magnitude larger than single crystals) [5, 6]. The absorption at low photon energies could also be increased by over one order of magnitude by lithographically texturing the single crystals [7]. This observed sub-bandgap absorption was attributed to energy levels within the bandgap arising from edge

states. [5–7].

Recently, there has been renewed interest in MoS₂, and re-examination and extension of earlier studies into the fundamental properties of MoS₂ monolayers, with a focus on leveraging their promising characteristics for new photonic technologies. In particular, MoS₂-based devices have been used as passive optical switches for short-pulse generation by the well-established mechanisms of mode-locking and Q-switching [10–19]. Few-layer and monolayer MoS₂ samples have been shown to possess a high third-order nonlinear susceptibility [20] and ultrafast carrier dynamics [21], suggesting their suitability as a fast saturable absorber (SA). Indeed, saturable absorption behaviour in MoS₂ was verified experimentally in 2013 by Wang *et al.* [10]. Such nonlinear absorption at photon energies sufficient to traverse the material bandgap arises due to Pauli blocking, where under intense illumination energy levels in the conduction band are filled, and further absorption is blocked according to the Pauli exclusion principle [11].

There are, however, also reports of MoS₂ saturable absorption behaviour at longer wavelengths, corresponding to sub-bandgap photon energies [11, 12]. We recently reported Q-switching of a fixed-wavelength fiber laser at 1068 nm [19] using a few-layer MoS₂ saturable absorber. Similar approaches have been used to mode-lock a fiber laser at 1060 nm [13, 14] and 1550 nm [15–17], and to Q-switch solid-state lasers at 1060, 1420 and 2090 nm [18]. However, these reports are all at fixed laser wavelengths and pulse generation over a continuous wavelength range using few-layer MoS₂ has yet to be demonstrated (addendum: during the review process, a tunable Q-switched fiber laser using few-layer MoS₂ was published [22], although based on erbium-doped fiber, rather than ytterbium-doped fiber, as reported here.). For many applications such as spectroscopy and biomedical diagnostics, pulse sources with a tunable wavelength are required. We also note that few of the reports in literature comment on the fact that their laser wavelength is below the MoS₂ material bandgap, and the saturable absorption mechanism in this situation is not fully understood. We argue that this wideband saturable absorption below the material bandgap can be attributed to saturation of edge states, which arise from large edge to surface area ratios of few-layer MoS₂ flakes. [5, 18, 23]. This is supported by reports of pulse generation by saturation of defect states within the bandgap in other nonlinear optical crystals, such as chromium-doped garnets [24] and gallium arsenide [25]. We also note that a very recent study reported strong second-order nonlinear optical susceptibility enhancement from the atomic edge states of a MoS₂ monolayer [23]. While saturable absorption is a third-order nonlinear effect, the suggested variation in electronic structure at atomic edges is also consistent with our proposed mechanism.

To produce mono- and few-layer MoS₂, it is necessary to either exfoliate from bulk crystals, or to directly grow individual layers [26]. For fundamental studies and device fabrication, scotch-tape assisted mechanical cleavage and chemical vapour deposition (CVD) [27–29] are often preferred, producing high quality flakes. On the other hand, solution-based exfoliation – either chemically [3, 30] or ultrasound-assisted liquid phase exfoliation (LPE) [19, 31] – presents opportunities for large-scale production of few-layer and mono-layer flakes under ambient conditions. The resultant dispersions can be fabricated into composites by blending with polymers [19, 31], filtered to form films [31] and printed or coated onto arbitrary substrates [32]. Therefore, solution-based exfoliation represents an ideal device fabrication method for MoS₂-based SAs.

Here, we fabricate a free-standing MoS₂-polymer composite SA by LPE of MoS₂ bulk crystals into few-layer MoS₂ flakes and integrate these flakes into a polyvinyl alcohol (PVA) host. This composite is used in a fully fiber-integrated Q-switched laser, tunable over 40 nm, confirming the wideband saturable absorption of MoS₂. We explain the mechanism of saturable absorption at sub-bandgap wavelengths in the context of early studies [5–7], which highlighted the role of edge states.

2. MoS₂-PVA composite saturable absorber fabrication

The LPE process of MoS₂, similar to other layered materials, is a two step process [31]. First, chemically pristine bulk MoS₂ crystals are mixed with a solvent [31]. Second, ultrasound is used to induce local pressure variations, overcoming the weak interlayer van der Waals forces in the bulk crystals and producing a dispersion enriched in mono- and few-layer flakes [19,31]. Since the process involves no chemical pre- or post-treatment of the bulk crystal, the dispersed flakes are chemically pristine [31,33–36].

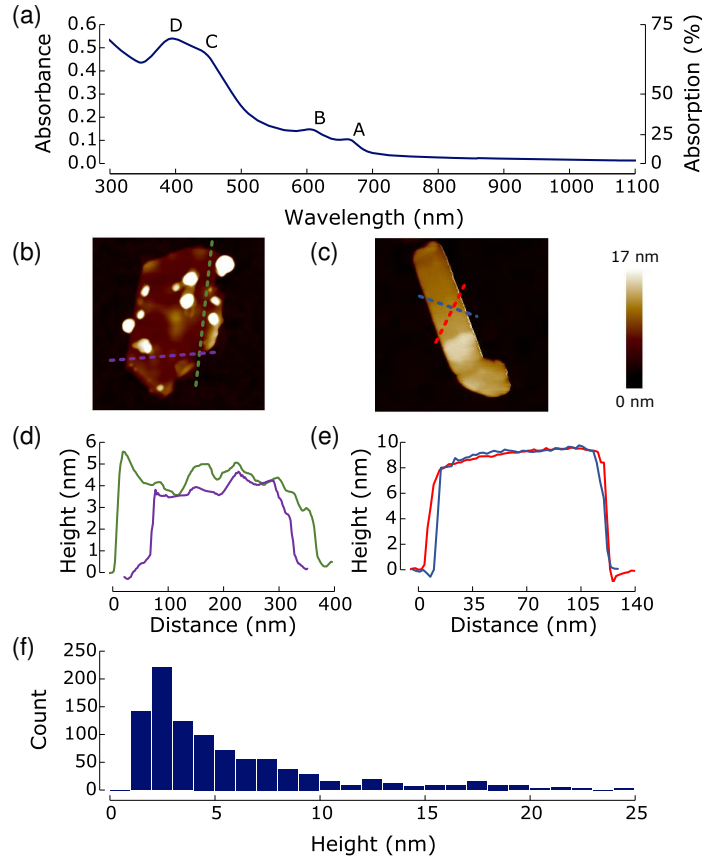


Fig. 1. Characterization of the dispersed MoS₂ flakes. (a) Optical absorption of dispersed MoS₂. (b-f) Characterization via AFM: (b-e) images of typical flakes and flake thickness profiles, (f) distribution of flake thicknesses.

Suitable solvents for exfoliation of LPE flakes are those with a similar solvent surface energy to the dispersed material [31, 35], typically in the range of $\sim 70 \text{ mJ m}^{-2}$ (MoS₂ $\sim 75 \text{ mJ m}^{-2}$ [33], graphite/graphene $\sim 70 \text{ mJ m}^{-2}$ [36]). An example is *N*-methyl-pyrrolidone (NMP), which is widely used to disperse graphene [35, 37, 38] and MoS₂ [31, 33]. However, its high boiling point (202 °C) can present processing challenges. For low-temperature applications, water is the preferable solvent. In this case, it is necessary to use a dispersant such as surfactant or polymer [34, 35], as the surface energy of water ($\sim 100 \text{ mJ m}^{-2}$ [39]) is too far from that of MoS₂ to support exfoliation and stabilization. We use a bile salt surfactant, sodium deoxycholate (SDC) to exfoliate and stabilize MoS₂. SDC has a flat molecular structure and a hydrophobic and a hydrophilic side and therefore, is better suited for exfoliation of 2D mate-

rials [35]. The hydrophobic side of the molecule adsorbs onto the surface of the flake, while the hydrophilic side provides Coulomb repulsion between adjacent flakes, preventing reaggregation [35]. To prepare the MoS₂ dispersion, we ultrasonicate 120 mg of MoS₂ crystals (Acros Organics, 6 μm) with 90 mg SDC in 10 mL deionized water for 2 hours at ~5 °C. We then centrifuge the dispersion at ~4,200g in a swinging bucket rotor for 1 hour. Larger flakes and less exfoliated material sediment faster through the centrifuge cell, leaving the upper 80% of the dispersion containing primarily few- and mono-layer flakes. This is then collected for analysis and composite fabrication.

The concentration of the dispersed MoS₂ can be estimated from the optical absorption of the dispersion [31] via the Beer-Lambert law: $A_\lambda = \alpha_\lambda cl$, where A_λ the absorption at wavelength λ , α_λ is the absorption coefficient ($\text{L g}^{-1} \text{m}^{-1}$), l is the absorption length (m) and c is the concentration (g L^{-1}). The optical absorption of the MoS₂ in the dispersion, diluted to 10 vol%, is shown in Fig. 1(a). The four peaks in the absorption spectrum result from the A (~665 nm) and B (~605 nm) excitonic transitions, and the C (~440 nm) and D (~395 nm) transitions between regions of the band structure with higher density of states [40, 41]. The concentration is estimated from the absorption at three wavelengths; using $\alpha_{605} = 1583 \text{ L g}^{-1} \text{m}^{-1}$, $\alpha_{665} = 1284 \text{ L g}^{-1} \text{m}^{-1}$, and $\alpha_{800} = 324 \text{ L g}^{-1} \text{m}^{-1}$ we calculate a MoS₂ concentration of ~0.08 g L^{-1} .

The dispersed flakes are then characterized by atomic force microscopy (AFM). The dispersion is further diluted to 5 vol% and drop-cast onto a Si/SiO₂ wafer. The sample is then rinsed with deionized water to remove residual surfactant. This allows isolated flakes to be imaged with an AFM, using a silicon cantilever with a silicon nitride tip. AFM images of typical flakes are shown in Figs. 1(b) and 1(c), along with their height profiles in Figs. 1(d) and 1(e). The distribution of flake thicknesses [Fig. 1(f)] reveals that 48% fall into the range 2-4 nm, corresponding to ~4-5 layers, assuming ~1 nm measured thickness for a monolayer flake and ~0.7 nm increase for each additional layer [42]. The lateral dimensions of flakes are found to be ~100-200 nm.

The SA composite film is fabricated by mixing 4 mL of ~0.08 g L^{-1} MoS₂ dispersion with 2 mL of 15 wt% aqueous polyvinyl alcohol (PVA) solution. The mixture is dried in a petri-dish at ~20°C, forming a ~25 μm thick free-standing composite film.

3. MoS₂-PVA composite saturable absorber characterization

We verify the quality of the MoS₂-PVA composite film by using optical microscopy, as shown in Fig. 2(a), and scanning electron microscopy (SEM), shown in Fig. 2(b) [43]. The SEM image (captured with an FEI Magellan SEM) shows the film in cross-section, following slicing with a Leica Ultracut UCT. Both images confirm the absence of >1 μm aggregates or voids in the composite SA, which could otherwise result in non-saturable scattering losses [44]. The linear optical absorption of the composite film is shown in Fig. 2(d), in addition to the absorption of a pure PVA sample of equivalent thickness for comparison. The absorption is uniform within the operating range of the tunable Q-switched laser we report here (shaded in blue). The pure PVA sample absorbs ~8% (0.04 absorbance) whereas the MoS₂-PVA composite absorbs ~24% (0.12 absorbance). This suggests that MoS₂ flakes in our sample are responsible for the increased value of absorbance, confirming absorption of light (assuming negligible scattering contribution) in the near-infrared region corresponding to photon energies below the MoS₂ bandgap.

The nonlinear properties of our MoS₂ saturable absorber are characterized using open-aperture Z-scan measurements [45]. The MoS₂-PVA composite is moved through the focal plane of a beam of ultrashort pulses (500 fs pulse duration, 26.4 MHz repetition frequency, 1065 nm wavelength) and the transmitted power (and also a reference power for normalization) are recorded, as shown in Fig. 2(c). With increasing peak intensity, the material absorption de-

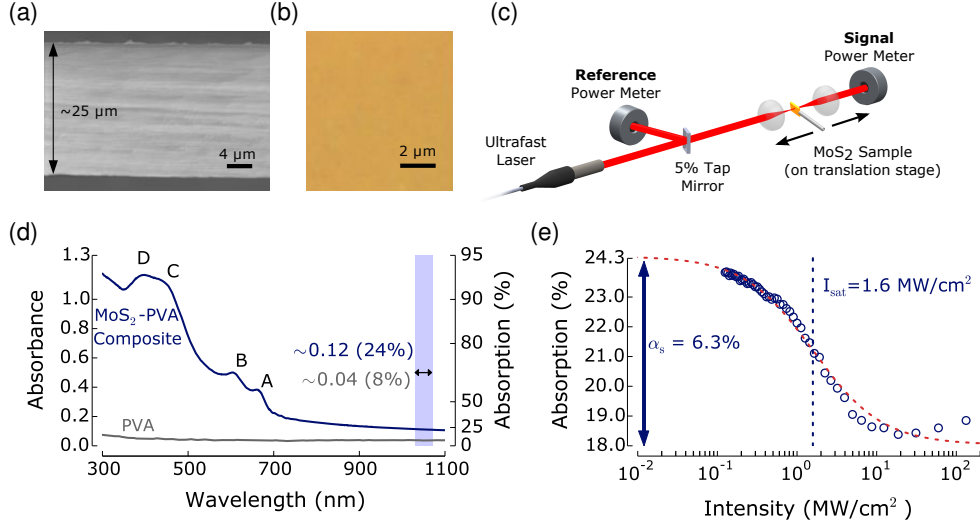


Fig. 2. Characterization of the MoS₂-polymer SA film. (a) SEM of the cross-section and (b) optical micrograph confirming the absence of aggregates. (c) Z-scan setup. (d) Optical absorption of the film, with the highlighted region indicating the range of operation of the tunable Q-switched laser. (e) Nonlinear absorption profile showing saturable absorption.

creases [Fig. 2(e)], confirming saturable absorption. The intensity-dependent absorption, $\alpha(I)$, can be fitted by the standard two-level saturable absorber model [46]:

$$\alpha(I) = \frac{\alpha_s}{1 + I/I_{\text{sat}}} + \alpha_{\text{ns}} \quad (1)$$

where I is pump light intensity, I_{sat} is the saturation intensity, α_s and α_{ns} are the saturable (i.e. modulation depth) and non-saturable loss, respectively. From the fit we find: $\alpha_s \sim 6.3\%$, $\alpha_{\text{ns}} \sim 18\%$, and $I_{\text{sat}} \sim 1.6 \text{ MW cm}^{-2}$. Previous reports of few-layer MoS₂ SAs have measured $I_{\text{sat}}=2.45 \text{ GW cm}^{-2}$ and $\alpha_s=27\%$ at 1060 nm using pulsed laser deposited MoS₂ [18], $I_{\text{sat}}=0.35 \text{ MW cm}^{-2}$ and $\alpha_s=35.4\%$ at 1550 nm using CVD MoS₂ [15] and $I_{\text{sat}}=34 \text{ MW cm}^{-2}$ and $\alpha_s=4.3\%$ at 1550 nm using hydrothermal intercalated MoS₂ [16]. This wide variation could be attributed to the different fabrication techniques which determine the size and quality of the MoS₂ flakes, and hence the contribution to absorption from edge states in the bandgap [5–7]. We also note that our measured saturation intensity for few-layer MoS₂ is lower than commonly reported values for other nanomaterial saturable absorbers based on CNTs ($\sim 20 \text{ MW cm}^{-2}$ [43]) and graphene ($\sim 260 \text{ MW cm}^{-2}$ [37]), which could be beneficial for achieving pulse generation in fiber lasers.

4. Tunable Q-switched laser design and characterization

The nonlinear response of the saturable absorber can be used to modulate the loss and the Q-factor of a laser cavity to generate a regular train of Q-switched pulses. To achieve this, the MoS₂ saturable absorber is inserted into a fully fiber-integrated ring cavity (Fig. 3) by sandwiching a $\sim 1 \text{ mm} \times 1 \text{ mm}$ piece of the composite between angled patch cords. Angled connectors are used instead of flat connectors to minimize parasitic reflections. The cavity also consists of an ytterbium-doped fiber amplifier (IPG YAU-2-SL, with 1.5 m active fiber), a polarization-independent isolator to ensure unidirectional propagation, a 10% output coupler

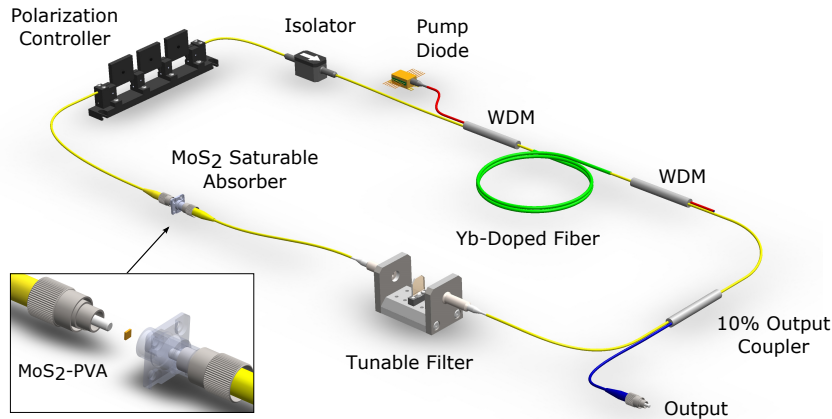


Fig. 3. Q-Switched fiber laser cavity schematic.

and a polarization controller. A tunable bandpass filter (formed of a fiber-coupled air gap with an angle-tunable bandpass interference filter) with 1 nm bandwidth is included to tune the lasing wavelength of the cavity. The total cavity length is ~ 13 m.

As the amplifier pump power is increased, the cavity initially lases in a continuous-wave regime. By further increasing the pump power, self-starting Q-switching is observed, producing a stable train of pulses. Typical output characteristics of the laser, at 1055 nm wavelength and 9.36 mW average output power, are shown in Fig. 4. Pulses are generated with 13.4 μs pulse spacing [Fig. 4(a)], corresponding to 74 kHz repetition rate, and a full width at half maximum (FWHM) pulse duration of 2.88 μs [Fig. 4(b)]. This corresponds to a pulse energy of 126 nJ. The radio-frequency (RF) spectrum of the output shows a high peak-to-background contrast of ~ 45 dB [Fig. 4(c)], indicating good pulse train stability [47], comparable to Q-switched fiber lasers based on graphene [48].

The average output power in the Q-switched regime is variable from 7.0 mW up to 10.5 mW, limited by the available pump power. The pulse properties in continuous-wave pumped Q-switched lasers depend on nonlinear dynamics in the gain medium and saturable absorber. This leads to a dependence of repetition rate and pulse duration upon pump power [49]. A pulse is emitted once a certain stored energy in the cavity is reached. Thus, a greater pump power enables higher repetition rates and also results in shorter pulses [49]. This was observed experimentally as the pulse duration is reduced from 4.40 μs to 2.68 μs and the repetition rate is increased from 65.3 kHz to 89.0 kHz with increasing output power [Fig. 4(d)]. The pulse duration could be shortened further by reducing the length of the laser cavity [49].

By varying the passband of the tunable filter, stable Q-switched operation is achieved with continuous tunability from 1030 nm to 1070 nm [Fig. 4(e)], producing a steady train of pulses. As the amplifier gain changes with wavelength, the output power of the laser varies. It is therefore necessary to adjust the pump power to maintain Q-switching; this accounts for the variations in spectral intensities in Fig. 4(e). We believe the tuning range is limited by the gain bandwidth of the ytterbium amplifier rather than the saturable absorber. Therefore, with a gain medium supporting broader band operation, we expect that tunable Q-switched laser pulses could be generated over an even wider spectral range.

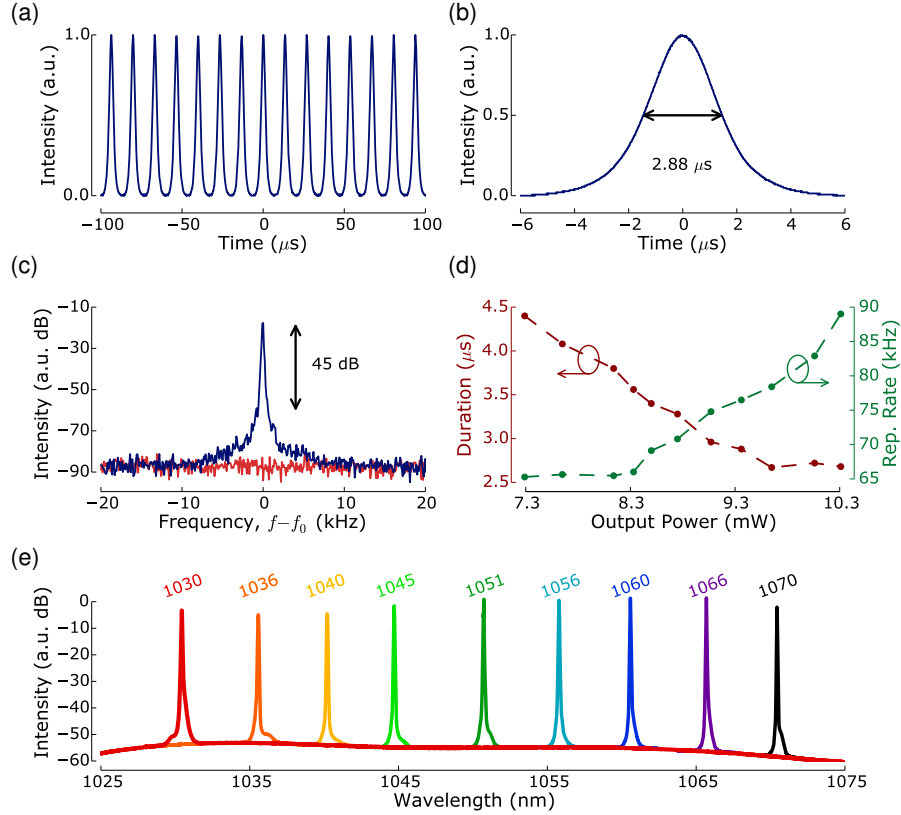


Fig. 4. Q-switched laser characteristics: (a) Pulse train. (b) Single pulse profile. (c) RF spectrum of fundamental frequency, $f_0=74$ kHz. (d) Variation of repetition frequency and pulse duration with output power. (e) Output spectra for Q-Switched operation at various wavelengths. The wavelength could be continuously tuned between 1030 and 1070 nm using the tunable filter.

5. Discussion

In a perfect crystalline lattice, the bandgap – corresponding to the energy range where no electron states can exist – prohibits absorption of single-photons that have an energy insufficient to excite electrons from the valence to the conduction band [8, 9]. Yet, our Z-scan measurements and experimental demonstration of Q-switching of a fiber laser using an MoS₂-PVA composite unequivocally confirm that the material exhibits saturable absorption at wavelengths in the range 1030-1070 nm (1.20-1.16 eV), despite corresponding to photon energies lower than the material bandgap. This phenomenon of sub-bandgap saturable absorption has also recently been reported by a number of other groups [10, 13, 15, 16, 18, 19]. Despite this growing body of work, a full explanation of the governing physical mechanism has yet to be formulated.

We attribute sub-bandgap saturable absorption in MoS₂ to the presence of edge states within the material bandgap that arise due to the boundaries of a finite crystal structure. The basal planes of MoS₂ crystals are known to be chemically inert due to tight bonding between the exposed S atoms with the Mo atoms underneath, and are thus expected to be optically inactive. However, we propose that the large edge to surface area ratio of few-layer nanoflakes of MoS₂ results in a large number of edge-sites, leading to the presence of energy states within the

pristine crystal band structure. We believe these edge states promote absorption at photon energies lower than the bandgap – an argument consistent with earlier studies [5–7]. We suggest that these states could then be saturated under high intensity illumination, due to the principle of Pauli blocking [8, 46]. It should also be noted that edge effects in few-layer MoS₂ have been related to enhanced second-order nonlinear optical processes, such as second harmonic generation [23], and as a route for fast intraband relaxation [50].

A distribution of edge states within the bandgap could explain the wideband saturable absorption experimentally observed here, and in other recent reports at a number of different laser wavelengths (1030–2090 nm), corresponding to a broad range of photon energies (1.20–0.59 eV) [13, 15, 16, 18, 19]. Finally, we envisage that this description of wideband saturable absorption at sub-bandgap photon energies should be applicable to other semiconducting mono- and few-layer transition metal dichalcogenides, such as WS₂, MoSe₂ and MoTe₂.

6. Conclusion

In summary, we have fabricated a few-layer MoS₂-PVA composite saturable absorber by liquid phase exfoliation. This device is used to Q-switch a fiber laser, with 40 nm of tunability, and producing pulses with over 100 nJ pulse energy, microsecond pulse durations and at tens of kilohertz repetition rates. This highlights the potential of few-layer MoS₂ as a wideband saturable absorber. We have proposed an explanation for the wideband sub-bandgap saturable absorption mechanism in the context of edge states. We thus anticipate few-layer transition metal dichalcogenides will offer further opportunities in other nonlinear photonic and optoelectronic applications.

Acknowledgments

EJRK acknowledges support from the Royal Academy of Engineering (RAEng), through a RAEng Fellowship, RCTH from EPSRC (EP/G037221/1), GH from a CSC Cambridge International Scholarship, and TH from the RAEng (Graphlex). The authors also acknowledge ThorLabs for access to their technical drawings.